Available online at www.sciencedirect.com
SCIENCE DIRECT
Journal of Sound and Vibration 297 (2006) 365–381
JOURNAL OF SOUND AND VIBRATION
www.elsevier.com/locate/jsvi

Dynamic analyses of a flexible quick-return mechanism by the fixed and variable finite-difference grids

Jih-Lian Ha[a,*], Jer-Rong Chang[b], Rong-Fong Fung[c]

[a]*Department of Mechanical Engineering, Far East College, 49 Chung-Hua Road, Shin-Shi, Tainan 744, Taiwan, ROC*
[b]*Department of Aircraft Engineering, Air Force Institute of Technology, 1 Jyulun Road, Gang-Shan, Kaohsiung 820, Taiwan, ROC*
[c]*Department of Mechanical and Automation Engineering, National Kaohsiung First University of Science and Technology, 1 University Road, Yenchau, Kaohsiung 824, Taiwan, ROC*

Received 2 December 2004; received in revised form 7 March 2006; accepted 10 April 2006
Available online 16 June 2006

Abstract

The finite difference method (FDM) with fixed and variable grids is proposed to approximate the numerical solutions of a flexible quick-return mechanism. In the dynamic analysis and simulation, the flexible rod is divided into two regions. Each region with time-dependent length is modeled by Euler-beam theory. Sufficient stability and convergence conditions are established for these finite difference schemes. It is found that for the fixed-grid method, numerical divergence occurs when the moving boundary moves across any of the neighboring nodes. The possibility of break down can be avoided via the variable-grid method, in which a coordinate transformation is employed to fix the moving boundary. Numerical results are discussed and provided to justify the stability and convergence.

1. Introduction

The traditional approach to dynamic analysis of mechanisms and machines usually makes the assumption that the systems are composed of rigid bodies. However, when a mechanism operates at a high-speed condition, the rigid-body assumption is no longer valid and the links should be considered flexible. In the quick-return mechanism, since the translating/rotating joint moves reciprocally along the flexible rod, the rod is divided into two regions with time-dependent length. Many numerical methods, such as the finite-element method (FEM) and Galerkin's method, have been used to solve the problem with time-dependent domain.

The brief review of the numerical analysis about the system with time-dependent domain is as follows. First, for systems with time-dependent domain by Galerkin's method, Dwivedi [1] presented approximate expressions for the angular displacement, velocity and acceleration of the mechanism. The quick-return mechanism was investigated by Beale and Scott [2,3] on the deflection and stability, whereas the rod was considered as an Euler–Bernoulli beam. Spatial dependence was eliminated by using Galerkin's method with time-dependent pinned–pinned overhanging beam modes. Okuyiga and Ray [4] solved numerically the

*Corresponding author. Tel.: +886 6 5977105; fax: +886 6 5977100.
E-mail address: jackha@cc.fec.edu.tw (J.-L. Ha).

0022-460X/$ - see front matter © 2006 Elsevier Ltd. All rights reserved.
doi:10.1016/j.jsv.2006.04.005

displacement of a slightly compressible liquid for the 1D case. Fung and Cheng [5] approximated a string/slider system by using Galerkin's method with time-dependent basis functions. Lee [6] presented the dynamics of a flexible rod of a quick-return mechanism. In general, Galerkin's approach is computationally too intensive due to the time-dependent boundary and its complex mode shape.

Second, for systems with time-dependent domain by the FEM, many works on the dynamics and stability of a flexible rod in a quick-return mechanism were based on the FEM. For examples, Bahgat and Willmert [7], Song and Haug [8] and Yang and Sadler [9] employed the FEM in their works to investigate the dynamics of the flexible planar mechanisms. Fung and Lee [10] investigated the stability of a quick-return mechanism with time-dependent coefficients. The flexible multibody machine tool mechanism subjected to constant and chattering cutting forces was analyzed by Shabana and Thomas [11]. Fung and Chen [12] simulated the flexible rod of a quick-return mechanism driven by a PM synchronous servomotor by the FEM. A variable-domain beam finite element with the size being a prescribed function of time was formulated by Stylianou and Tabarrok [13]. For a translating and rotating beam, a transition finite element with variable stiffness introduced at the interface of the joint hub was addressed in Refs. [14,15]. Generally speaking, the advantage of FEM is its ability to handle complex geometry; however, it requires more CPU time and is less suitable to vectorization and parallel computation than the finite difference method (FDM) [16,17].

Finally, are systems with time-dependent domain by the FDM, which is the most popular choice for numerical solutions in the moving boundary problems. Kharab [18] demonstrated the use of a spreadsheet program that simulates the location of a moving boundary of the one-phase Stefan problem. By using the FDM, the idea of a coordinate transformation to fix a moving boundary was used numerically [19,20]. Most studies of the system with time-dependent domain solved numerically by the FDM focused on the solidification/melting and Stefan problems. To the authors' knowledge, there are very few papers investigating the flexible planar mechanisms by use of the FDM.

The main objective of this paper focuses on the application of the FDM to dynamic analysis of the flexible quick-return mechanism. The FDM with the fixed- and variable-grid methods is employed and the stability and convergence conditions for these finite difference schemes are established. The variable-grid method based on coordinate transformation, which transforms the time-varying domain into a constant one, is found to be the most suitable for the quick-return mechanism with moving boundary.

2. Formulations of physical model

The undeformed configuration of the flexible quick-return mechanism is shown in Fig. 1. The mechanism consists of the rigid crank AJ with length r, the rigid rod BC with length D, the flexible rod OB with length L, and the slider C with mass m_c. Other symbols are as follows: F, external force acting on the slider; θ, crank angle; ϕ, angle between the Y-axis and the rigid-body reference axis of the flexible rod OB; β, angle between the X-axis and the rigid rod BC.

The deformed configuration of the quick-return mechanism is shown in Fig. 2. $\mathbf{e}_i$ and $\mathbf{e}_j$ are the unit vectors of the rotating frame Oxy which rotates with an angular speed $\dot{\phi}$. $\mathbf{i}$ and $\mathbf{j}$ are the unit vectors of the fixed frame OXY. $x_1(t)$ is the current position of the translating/rotating joint. The frictional forces at the translating/rotating joint and slider C are neglected. The dimension of the slider J compared with the flexible rod is small and thus for simplicity is considered to be massless and treated as a point [10,12]. The flexible quick-return mechanism considered in this paper, which includes the rigid rod BC and slider C, is different from those in Fung and Lee [10], Lee [6] and Beale and Scott [2] where the above parts were not considered.

For the sake of convenience the following differential notations are used: $()' = \partial()/\partial x$ and $(\bullet) = \partial()/\partial t$. If the slenderness ratio is very small, the shear deformation can be neglected in comparison with the flexural deformation, and Euler-beam theory can be used to describe the motion of the flexible rod. The displacement field of any point P of the flexible rod before deformation is

$$u_1(x, y, t) = -yv'(x, t),$$
$$u_2(x, y, t) = v(x, t), \tag{1}$$

where v represents the transverse displacement of the flexible rod.

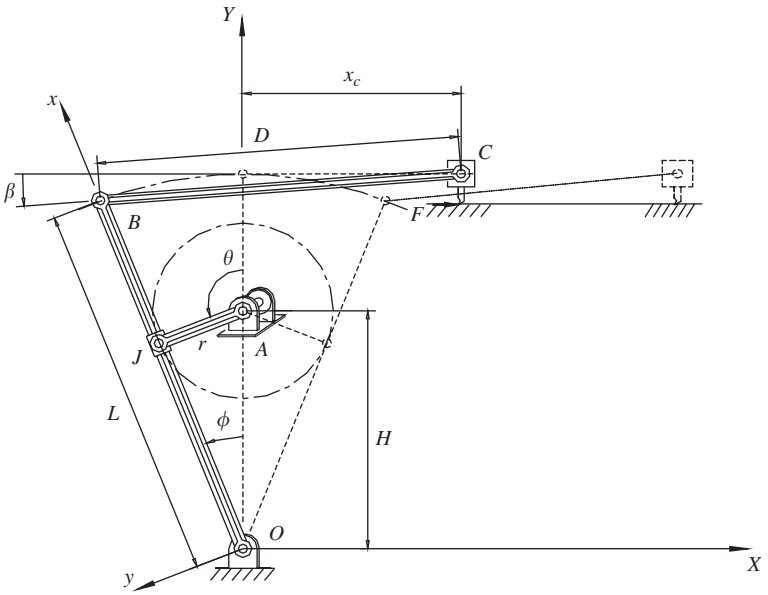

Fig. 1. Quick-return mechanism before deformation.

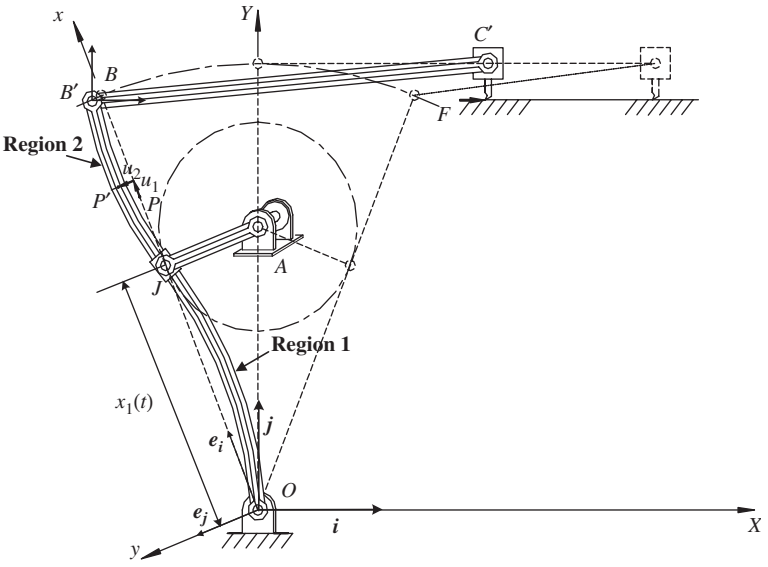

Fig. 2. Deformed quick-return mechanism with a flexible connecting rod.

In this paper, the rotating coordinate system Oxy fixed on the flexible connecting rod is selected to be the reference coordinate. Fig. 2 shows the flexible rod undergoing gross motion and elastic deformation. The deformed position vector of an arbitrary point P is

$$\mathbf{R}(x, y, t) = (x + u_1)\mathbf{e_i} + u_2\mathbf{e_j}. \tag{2}$$

By differentiating Eq. (2) with respect to time t, the absolute velocity is

$$\mathbf{R}_t(x, y, t) = \left(-y\dot{v}' - v\dot{\phi}\right)\mathbf{e_i} + \left((x - yv')\dot{\phi} + \dot{v}\right)\mathbf{e_j}. \tag{3}$$

The total kinetic energy is the sum of the flexible rod OB, rigid rod BC, crank AJ and slider C. The kinetic energy of the flexible rod OB is expressed as the sum of two regions of integration:

$$T_{OB} = \frac{1}{2}\left(\int_0^{x_1^-(t)} + \int_{x_1^+}^{L}\right)\left\{\rho A\left\{v^2\dot{\phi}^2 + \left[x\dot{\phi} + \dot{v}\right]^2\right\}\right\} \mathrm{d}x. \tag{4}$$

If the mass of the slider J is considered, the associated kinetic energy has to be added to the formulation. It is neglected in this study. The kinetic energy of crank with mass m_{AJ} and moment of inertia I_{AJ} is

$$T_{AJ} = \frac{1}{2} I_{AJ}\dot{\theta}^2 = \frac{1}{6} m_{AJ} r^2 \dot{\theta}^2. \tag{5}$$

The kinetic energy of the rigid rod BC with mass m_{BC} and moment of inertia I_{BC} is

$$T_{BC} = \frac{1}{2}\left(m_{BC}\dot{X}_{BC}^2 + m_{BC}\dot{Y}_{BC}^2 + I_{BC}\dot{\beta}^2\right), \tag{6}$$

where

$$X_{BC} = -L\sin\phi + \frac{D}{2}\cos\beta - u_L\sin\phi - v_L\cos\phi,$$
$$Y_{BC} = -\frac{D}{2}\sin\beta + u_L\cos\phi - v_L\sin\phi,$$
$$I_{BC} = \frac{1}{12} m_{BC} D^2.$$

The kinetic energy of the slider C with mass m_c is

$$T_C = \frac{1}{2} m_C \dot{X}_C^2, \tag{7}$$

where $X_C = D\cos\beta - L\sin\phi - v_L\, vos\,\phi$, and $v_L(= v(L,t))$ denotes the displacement at the end of the flexible rod.

The Lagrange strains are

$$\varepsilon_{xx} = -yv'', \quad \varepsilon_{yy} = \varepsilon_{xy} = 0, \tag{8}$$

where the high order terms $\frac{1}{2}v'^2$ and $yv'v''$ are neglected. The strain energy U of the system resulting from the bending deformation of the flexible rod is also expressed as the sum of two spatial integrals:

$$\begin{aligned} U &= \frac{1}{2}\int_V \sigma_{ij}\varepsilon_{ij}\,\mathrm{d}V, \\ &= \frac{1}{2}\left(\int_0^{x_1^-(t)} + \int_{x_1^+}^{L}\right)\left\{EIv''^2\right\}\mathrm{d}x. \end{aligned} \tag{9}$$

The virtual work done by the external force F applied on the slider is

$$\begin{aligned} \delta W &= F\delta X_C \\ &= -F\cos\phi\,\delta v_L. \end{aligned} \tag{10}$$

Hamilton's principle for the flexible quick-return mechanism is

$$\int_{t_1}^{t_2} (\delta T_{\text{total}} - \delta U + \delta W)\,\mathrm{d}t = 0, \tag{11}$$

where $T_{\text{total}} = T_{BO} + T_{BC} + T_{AJ} + T_c$. By substituting Eqs. (4)–(10) into Eq. (11) and taking variations, one obtains the governing equation of the transverse deflection for flexible rod:

$$\rho A\left(\ddot{v} + x\ddot{\phi} - v\dot{\phi}^2\right) + EIv'''' = 0, \quad 0 < x < x_1^-, \quad x_1^+ < x < L \tag{12a, b}$$

and the boundary conditions are

$$v(0,t)=0,\quad v''(0,t)=0,\quad v(x_1^-,t)=0,\quad v(x_1^+,t)=0, \tag{13a–d}$$

$$v'(x_1^-,t)=v'(x_1^+,t),\quad v''(x_1^-,t)=v''(x_1^+,t),\quad v''(L,t)=0, \tag{13e–g}$$

$$\begin{aligned} &m_{BC}[L\dot{\phi}^2\cos\phi\sin\phi+v_L\dot{\phi}^2-\frac{1}{2}D\dot{\beta}^2\cos(\phi+\beta)-\frac{1}{2}D\ddot{\beta}\sin(\phi+\beta)\\ &-\ddot{v}_L-L\ddot{\phi}\cos^2\phi]+m_C[L\dot{\phi}^2\sin\phi\cos\phi-D\dot{\beta}^2\cos\beta\cos\phi\\ &-D\ddot{\beta}\sin\beta\cos\phi-L\ddot{\phi}\cos^2\phi+v_L\dot{\phi}^2\cos^2\phi+v_L\ddot{\phi}\sin\phi\cos\phi\\ &+3\dot{v}_L\dot{\phi}\cos\phi\sin\phi-\ddot{v}_L\cos^2\phi]+EIv_L'''-F\cos\phi=0. \end{aligned} \tag{13h}$$

It is seen that the rigid-body motion and flexural vibration are coupled. The part of the flexible rod inside the rigid slider is treated as only one point. The translating/rotating joint is treated as a knife edge so that it can be assumed that the displacement, slope and curvature of the flexible rod are continuous across the translating/rotating joint, and these continuous conditions are seen in boundary conditions (13c–f). The boundary condition (13h) represents the force equilibrium at the end point of the flexible rod.

The kinematics of the mechanism is assumed that the crank is driven by a servomotor at a constant angular speed $\dot{\theta}$. Thus, the mechanism is of one degree-of-freedom (dof). The functions ϕ, x_1 and their derivatives can be expressed in terms of the known parameters θ and $\dot{\theta}$ as

$$\begin{aligned} &\phi=\sin^{-1}\left(\frac{r\sin\theta}{(r^2+H^2+2rH\cos\theta)^{1/2}}\right),\quad \dot{\phi}=\frac{r\dot{\theta}\cos(\theta-\phi)}{x_1},\\ &\ddot{\phi}=\frac{rH\dot{\theta}^2(r^2-H^2)\sin\theta}{x_1^4}, \end{aligned} \tag{14a–c}$$

$$\begin{aligned} &x_1=(r^2+H^2+2rH\cos\theta)^{1/2},\quad \dot{x}_1=\frac{-rH\dot{\theta}\sin\theta}{x_1},\\ &\ddot{x}_1=\frac{-x_1rH\dot{\theta}^2\cos\theta+\dot{x}_1rH\dot{\theta}\sin\theta}{x_1^2}. \end{aligned} \tag{15a–c}$$

From the geometric relationships, the angle β and its derivatives can be expressed in terms of ϕ as

$$\begin{aligned} &\beta=\sin^{-1}\left(\frac{L(1-\cos\phi)}{D}\right),\quad \dot{\beta}=\frac{L\dot{\phi}\sin\phi}{D\cos\beta},\\ &\ddot{\beta}=\frac{L\ddot{\phi}\sin\phi+L(\dot{\phi})^2\cos\phi+D(\dot{\beta})^2\sin\beta}{D\cos\beta}. \end{aligned} \tag{16a–c}$$

It is seen that the functions ϕ, x_1, β and their time derivatives can be obtained, once the driving angle θ and angular speed $\dot{\theta}$ are known.

3. Finite difference schemes

The technique of finite difference method for the flexible quick-return mechanism with a translating/rotating joint will be introduced in this section. Previous works on the numerical results of a flexible rod of the quick-return mechanism are based on the FEM [10,12] and Galerkin's approximation [2,3] with time-dependent basis function. Here, two kinds of finite difference schemes associated with the fixed- and variable-grid methods are addressed for simulating the dynamic behavior of the system.

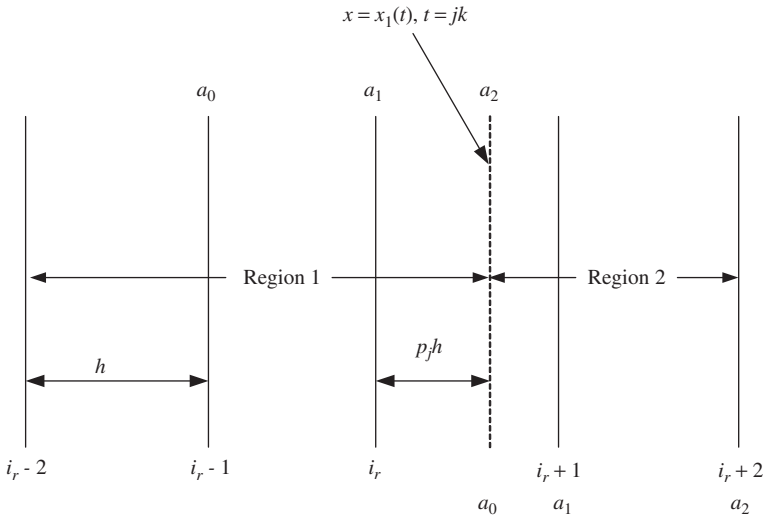

Fig. 3. Schematic of the moving boundary near the fixed grids at time jk.

3.1. Fixed-grid method

In order to approximate the partial differential equations by using the finite difference equations, the total length L is divided into N_f subdivisions. Let h and k be, respectively, the space and time discretization mesh sizes and let v_i^j denote the value of v at the ith node and jth time. A major difficulty arises due to the presence of unequal space interval near the moving boundary by using the FDM. Thus, the treatment of the nodes near the moving boundary is different from the other nodes. At any time jk, the most general case of the moving boundary $x_1(t)$ will usually be located between two neighboring grid points, denoted $i_r h$ and $(i_r + 1)h$, as shown in Fig. 3. This will be approximated by using the modified finite difference scheme, which incorporates unequal space interval near the moving boundary.

Lagrange interpolation is employed to solve the transverse displacements at the nodes near the moving boundary. Three-point formulae [17] for the general function $f(x)$, which has known values $f(a_0)$, $f(a_1)$ and $f(a_2)$ at the three points a_0, a_1 and a_2 respectively, is established as

$$f(x) = \sum_{i=0}^{2} \zeta_i(x) f(a_i), \tag{17}$$

where

$$\zeta_i(x) = \frac{\Gamma(x)}{(x - a_i)\Gamma'(a_i)}, \quad \Gamma(x) = (x - a_0)(x - a_1)(x - a_2).$$

Then the derivative terms of $f(x)$ can be easily derived. Fig. 3 shows the moving boundary at time jk, and at a fractional distance $p_j h$ between the grid line $i_r h$ and $(i_r + 1)h$. In region 1, the points a_0, a_1 and a_2 are identified with the grid lines, $(i_r - 1)h$, $i_r h$ and the moving boundary itself. The functions $f(a_0)$, $f(a_1)$ and $f(a_2)$ correspond to $v_{i_r-1}^j$, $v_{i_r}^j$ and v_B^j at the boundary, respectively. The treatments for the region 2 are similar with the region 1. The transverse displacements at the points near the moving boundary are detailed in Appendix A.

In summary, this method proceeds as follows:

Step 1: Given p_j and v_i^j to calculate v_i^{j+1}, $i = 0, 1, \ldots, i_r - 2$ and $i_r + 3, \ldots N_f$.

Step 2: Calculate $v_{i_r-1}^{j+1}$, $v_{i_r}^{j+1}$, $v_{i_r+1}^{j+1}$, and $v_{i_r+2}^{j+1}$ from Appendix A.

Step 3: Calculate p_{j+1}.

Step 4: Repeat steps (1)–(3) until the last time.

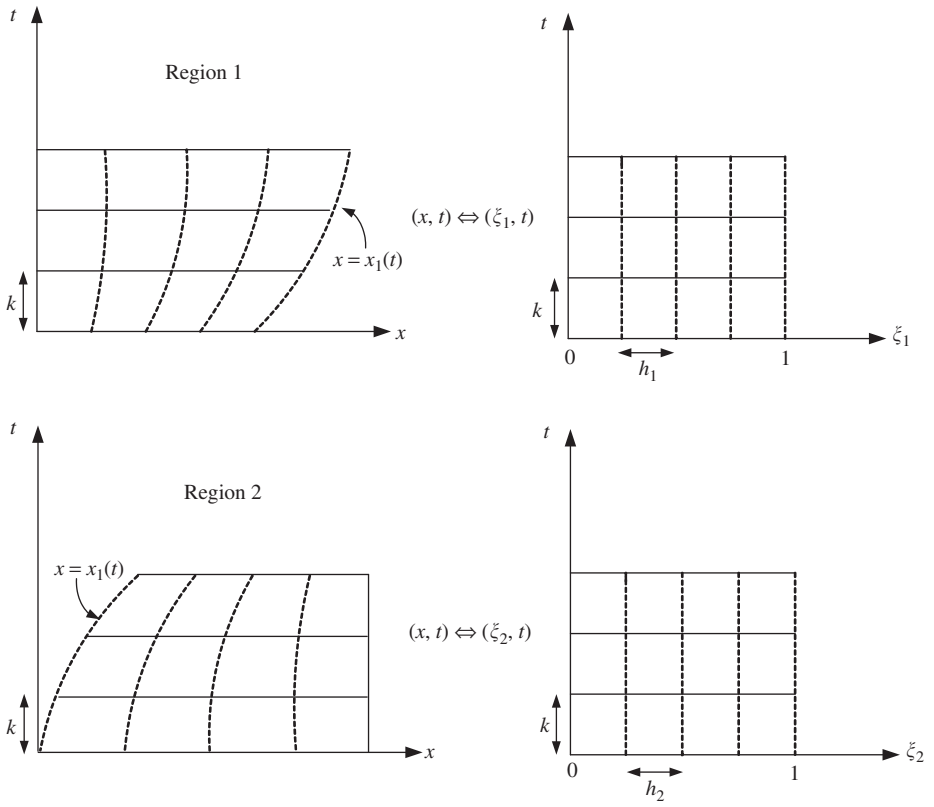

Fig. 4. Transformation to rectangular mesh for using variable-grid method.

3.2. Variable-grid method

Several techniques [19,20] of modifying the grid have been proposed in the variable-grid network, all with the intent to avoid the increased complication and the loss of accuracy associated with unequal intervals near the moving boundary. Since the translating/rotating joint moves reciprocally along the flexible rod, there is a time-dependent boundary involved. By using the variable-grid method, the original grid system (x,t) is transformed into a new system (ξ,t), which is orthogonal and is shown in Fig. 4. The total length L of the flexible rod is divided into two regions. The total number of space intervals between $x = 0$ and $x = L$ is constant and equals to N_v for the finite difference analysis. Regions 1 and 2 have n and m subdivisions, respectively. Thus, the total number of subdivisions N_v equals $m + n$.

In region 1, $0 \leqslant x \leqslant x_1^-(t)$, the moving boundary can be fixed by the coordinate transformation

$$\xi_1 = \frac{x}{x_1(t)}, \tag{18}$$

so that the moving boundary $x = x_1$ becomes $\xi_1 = 1$. The coordinate transformation for region 2 is

$$\xi_2 = \frac{x - x_1(t)}{L - x_1(t)}, \tag{19}$$

so that the moving boundary $x = x_1$ becomes $\xi_2 = 0$ and the end $x = L$ becomes $\xi_2 = 1$. Thus, the space intervals $h_1 = 1/n$ and $h_2 = 1/m$ in the regions 1 and 2, respectively, are proceeded in each time step. The moving boundary is always on the $(n+1)$th grid line in region 1 and the first grid line in region 2. A coordinate-transformation scheme is detailed in Appendix B for Euler-beam theory. It should be noted that the position x_1, speed $\dot{x}_1$ and acceleration $\ddot{x}_1$ of the moving boundary appear as coefficients in the transformed equations.

4. Stability and convergence analyses

The governing equation of the quick-return mechanism is a properly posed initial-value problem and the finite difference approximation satisfies the consistency condition. With the help of the lax equivalence theorem [21], stability analysis is necessary and sufficient for convergence in the finite difference scheme.

4.1. Fixed-grid method

Neglecting boundary conditions (13a–h), Von-Neumann stability analysis [21,22] is employed in the fixed-grid method. Denoting the actual machine printout as $\tilde{v}_i^j$, the round-off error is

$$e_i^j = v_i^j - \tilde{v}_i^j, \tag{20}$$

According to Eq. (12), both v_i^j and $\tilde{v}_i^j$ satisfy

$$v_i^{j+1} = 2v_i^j - v_i^{j-1} - k^2 x_i \ddot{\phi}_j + k^2 v_i^j \dot{\phi}_j^2 - \frac{a^2k^2}{h^4}\left(v_{i+2}^j - 4v_{i+1}^j + 6v_i^j - 4v_{i-1}^j + v_{i-2}^j\right), \tag{21a}$$

$$\tilde{v}_i^{j+1} = 2\tilde{v}_i^j - \tilde{v}_i^{j-1} - k^2 x_i \ddot{\phi}_j + k^2 \tilde{v}_i^j \dot{\phi}_j^2 - \frac{a^2k^2}{h^4}\left(\tilde{v}_{i+2}^j - 4\tilde{v}_{i+1}^j + 6\tilde{v}_i^j - 4\tilde{v}_{i-1}^j + \tilde{v}_{i-2}^j\right), \tag{21b}$$

where $a = \sqrt{EI/\rho A}$. And, subtracting, one can find that e_i^j satisfies

$$e_i^{j+1} = 2e_i^j - e_i^{j-1} + k^2 e_i^j \dot{\phi}_j^2 - \frac{a^2k^2}{h^4}\left(e_{i+2}^j - 4e_{i+1}^j + 6e_i^j - 4e_{i-1}^j + e_{i-2}^j\right). \tag{22}$$

Let $d_i^j = e_i^{j-1}$, the above three-level formula can be reduced to a two-level system as

$$\begin{aligned} e_i^{j+1} &= 2e_i^j - d_i^j + k^2 e_i^j \dot{\phi}_j^2 - \frac{a^2k^2}{h^4}\left(e_{i+2}^j - 4e_{i+1}^j + 6e_i^j - 4e_{i-1}^j + e_{i-2}^j\right), \\ d_i^{j+1} &= e_i^j. \end{aligned} \tag{23a, b}$$

Using a finite Fourier representation of the error e_i^j and d_i^j as

$$e_i^j = \sum_{m=0}^{N_f} E_m(j) \mathrm{e}^{\mathrm{i}m\pi x/L} = \sum_{m=0}^{N_f} E_m(j) \mathrm{e}^{\mathrm{i}m\pi i/N_f}, \tag{24a}$$

$$d_i^j = \sum_{m=0}^{N_f} D_m(j) \mathrm{e}^{im\pi x/L} = \sum_{m=0}^{N_f} D_m(j) \mathrm{e}^{im\pi i/N_f} \tag{24b}$$

where the symbol i means $\sqrt{-1}$. Substituting Eq. (24) into Eq. (23) and rearranging them to be the matrix form, we get:

$$\begin{Bmatrix} E_m(j+1) \\ D_m(j+1) \end{Bmatrix} = \begin{bmatrix} C & -1 \\ 1 & 0 \end{bmatrix} \begin{Bmatrix} E_m(j) \\ D_m(j) \end{Bmatrix}, \tag{25}$$

where $C = 2 + \dot{\phi}_j^2 k^2 - 16a^2k^2/h^4 \sin^4 \pi m/2N_f$. Since h and k are very small, the second term in C is much small than $O(1)$ and is omitted to simplify the following analysis. The eigenvalue λ of the 2×2 matrix in Eq. (25) can

be derived to satisfy the following equation

$$\lambda^2 - \left(2 - \frac{16a^2k^2}{h^4}\sin^4\frac{\pi m}{2N_f}\right)\lambda + 1 = 0. \tag{26}$$

If any of these eigenvalues are outside the unit circle for any x in the range $0 \leqslant x \leqslant L$, then the scheme is unstable. One wishes the roots of Eq. (26) to lie in or on the unit circle, hence one must have

$$\frac{16a^2k^2}{h^4}\sin^4\frac{\pi m}{2N_f} \leqslant 4. \tag{27}$$

Majorizing the left side of this inequality by replacing sine function by 1, one obtain a simple sufficient stability condition for the finite difference scheme as

$$\mu_f < 0.5, \tag{28}$$

where $\mu_f = ak/h^2$. Furthermore, a numerical divergence occurs when the moving boundary moves across any of the neighboring nodes. Since the value of p_j, as shown in Fig. 3, may be very close to be zero or unity, some equations in Appendix A become numerically divergent. The moving boundary needs to be located between two neighboring grind nodes, say node i_r and node $i_r + 1$. This situation depends on the geometry size of the mechanism. According to Fig. 1, the moving boundary position x_1 is located in the range $H - r \leqslant x_1 \leqslant H + r$ where the maximum and minimum values occur when the crank coincides with the driven rod. To have a convergent scheme, the subdivision number N_f must satisfy the following geometry constraints:

$$\frac{N_f(H+r)}{L} - 1 < i_r < \frac{N_f(H-r)}{L}. \tag{29}$$

It is noted that this equation is irrelevant to the time step k.

4.2. Variable-grid method

Following the process of previous subsection to apply Von-Neumann stability analysis, for region 1, the round-off errors e_i^j and d_i^j can be derived from the finite difference equation (B.1) as in Appendix B to get

$$\begin{aligned} e_i^{j+1} = {} & 2e_i^j - d_i^j + \frac{\xi_{1j}\dot{x}_{1j}k}{x_{1j}^2 h}\left(e_{i+1}^j - e_{i-1}^j - d_{i+1}^j + d_{i-1}^j\right) \\ & - \frac{\xi_{1j}^2\dot{x}_{1j}^2k^2}{x_{1j}^2h^2}\left(e_{i+1}^j - 2e_i^j + e_{i-1}^j\right) + \frac{\xi_{1j}(x_{1j}\ddot{x}_{1j} - 2\dot{x}_{1j}^2)k^2}{2x_{1j}^2 h}\left(e_{i+1}^j - e_{i-1}^j\right) \\ & + k^2 e_i^j\dot{\phi}_j^2 - \frac{a^2k^2}{x_{1j}^4h^4}\left(e_{i+2}^j - 4e_{i+1}^j + 6e_i^j - 4e_{i-1}^j + e_{i-2}^j\right), \end{aligned} \tag{30}$$

$$d_i^{j+1} = e_i^j. \tag{31}$$

For practical use and simplicity, the higher-order terms, the third to sixth terms of the right-hand side of Eq. (30), are neglected, and this can be justified by numerical examples. Using finite Fourier series expansion like Eq. (24a, b), one can derive a sufficient stability condition as

$$\frac{ak}{x_{1j}^2h_1^2} < 0.5. \tag{32}$$

One can take the following inequality as the sufficient stability condition

$$\mu_{v1} < 0.5, \tag{33}$$

where

$$\mu_{v1} = \frac{ak}{(H-r)^2 h_1^2}.$$

Similarly, for region 2, the sufficient stability condition is

$$\mu_{v2} < 0.5, \tag{34}$$

where

$$\mu_{v2} = \frac{ak}{(L-H+r)^2 h_2^2}.$$

It is sufficient to have a stable finite difference scheme for the variable-grid method if one chooses space and time increments, h_1, h_2 and k, to satisfy Eqs. (33) and (34) simultaneously.

5. Numerical results and dicussion

In the numerical results, we investigate two examples of the flexible quick-return mechanisms, which have the same material properties and dimensions as in Fung and Chen [12] and Fung and Lee [10]. The first example has the following dimensions and properties: $L = 1\,\text{m}$, $H = 0.59997\,\text{m}$, $r/H = 0.01$, $D = 1.2\,\text{m}$, $E = 0.7 \times 10^{11}\,\text{N/m}^2$, $I = 0.5208 \times 10^{-6}\,\text{m}^4$, $d = 0.05\,\text{m}$, $\rho A = 7.15\,\text{kg/m}$, $m_{BC} = 8.58\,\text{kg}$, $m_C = 0.5\,\text{kg}$. The second example has the following dimensions and properties: $L = 9.3746\,\text{in.}$, $H = 4.0\,\text{in.}$, $r = 1.5\,\text{in.}$, $EI = 2.91992 \times 10^6\,\text{lbfin}^2$, $\rho = 0.000725\,\text{lbin}^{-4}\,\text{s}^2$, $A = 0.4531\,\text{in.}^2$. The former belongs to the small crank of the quick-return mechanism while the later is the large crank.

5.1. The small crank case

The transverse deformations at the end point ($x = L$) of the rod, shown in Figs. 5 and 6, are obtained by applying the fixed-grid method and the variable-grid method, respectively, by taking $m_{BC} = m_C = 0$, i.e. the rigid link BC and slider C are not considered.

From the geometry constraint equation (29), it is obtained that the moving boundary moves across at least one of the neighboring nodes when the subdivision number is one of $N_f = 5$, 10, 15, 20, 25,30, 37, 38, 40, 42, 43, 45, 47, 48, 50, 52, 53, 55, 57, 58, 60, 62, 63, 65, and $N_f \geqslant 67$. This means that for this case the above values of N_f cannot be used in the finite difference scheme for the fixed-grid method since a numerical divergence is expected to occur. This is the main shortcoming for the fixed-grid method. Fig. 5a shows that the transverse displacements converge for larger values of N_f at time step $k = 5 \times 10^{-6}\,\text{s}$. From Table 1, it is reasonable to have the stable and convergent results since all satisfy the stability condition $\mu_f < 0.5$ shown in Eq. (28) for $N_f = 12$, 24, and 36. From Table 1, as the case with time step $k = 2 \times 10^{-6}\,\text{s}$, the stability condition $\mu_f < 0.5$ is satisfied for $N_f = 12$, 36, and 59, so the results shown in Fig. 5b are all stable and convergent. Comparison of Figs. 5a with b, it is seen that the numerical errors depend on the space step number N_f, and a larger value of N_f induces a less error. For a smaller time step, a larger value of N_f can be taken under the stability and geometry constraints.

Fig. 5c shows the divergent results when the value of N_f violates the geometry constraint, say $N_f = 10$ and 37 in this figure, in spite of the value of the time step. From Table 1, though $\mu_f = 0.4888$ for $N_f = 37$ satisfies the stability condition (28), numerical results are divergent since it violates the geometry constraint (29). Fig. 5d shows the divergent results due to the violation of the stability condition (28), from Table 1, say $\mu_f = 0.5155$ for $k = 5 \times 10^{-6}\,\text{s}$ and $N_f = 38$, and $\mu_f = 0.5141$ for $k = 2 \times 10^{-6}\,\text{s}$ and $N_f = 60$. It is seen from the comparison of Figs. 5c with d that the numerical results for the cases violating the stability condition (28) diverge far faster than those of violating the geometry condition (29). The transverse displacement for $k = 2 \times 10^{-6}\,\text{s}$ and $N_f = 60$ diverges faster than the other cases shown in Fig. 5c and d since it violates the stability condition and geometry condition simultaneously.

The transverse displacements at the end point, shown in Fig. 6, are obtained by using the variable-grid method. At $k = 5 \times 10^{-6}\,\text{s}$, $\mu_{v1} < 0.5$ and $\mu_{v2} < 0.5$ for $n = m = 3$, 6, 14, and $n = 22$ and $m = 14$, so that the

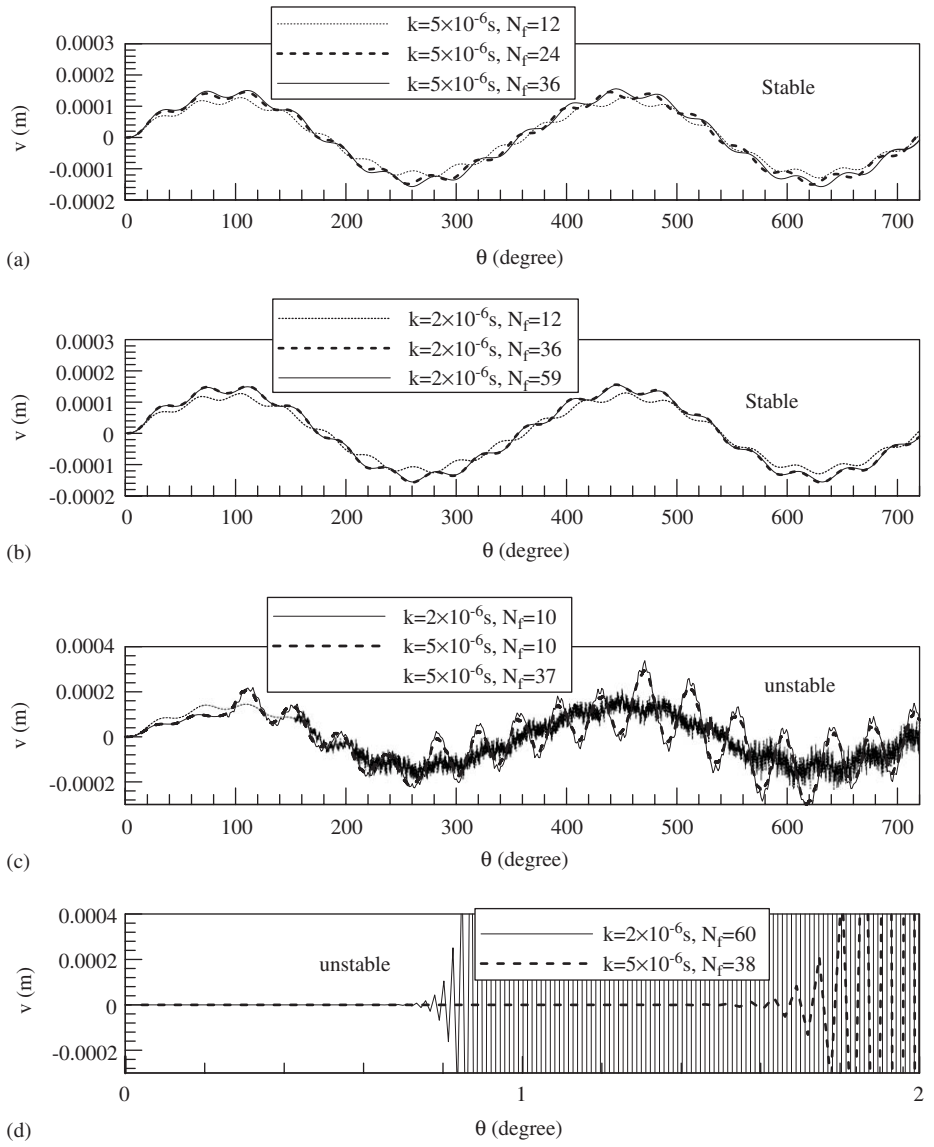

Fig. 5. Transverse deformations at the end point ($x = L$) with $m_{BC} = m_C = 0$ and $\dot{\theta} = 100\,\text{rad/s}$ by using the fixed-grid method.

numerical results of Fig. 6a are all stable and convergent. It is similar for $k = 2 \times 10^{-6}$ s, and the stable results are shown in Fig. 6b. Comparing of Figs. 6a with b, it is seen that the case for a smaller time step can be accompanied with a larger space step number. And a larger space step number brings about a less error.

From Table 2, it is obvious to see that the results shown in Fig. 6c are all unstable because any or all of the values of μ_{v1} and μ_{v2} exceed 0.5. Similarly, the results shown in Fig. 6d are also unstable with any or all of the values of μ_{v1} and μ_{v2} shown in Table 2 exceeding 0.5. It is also interesting to find that the stable cases for the fixed- and variable-grid methods have almost the same limit of the total subdivision number, N_f and N_v where $N_v = n + m$.

The comparison of the CPU time required solving the examples using the FDM with the comparable FEM is also investigated. As shown in Fig. 5a, the consumed CPU time to obtain the convergent curve by using the fixed-grid with $k = 5 \times 10^{-6}$ s and $N_f = 36$ is 41 s, whereas, for the variable-grid, from Fig. 6a, we see the convergent curve with $k = 5 \times 10^{-6}$ s and $n = m = 14$ is solved by consuming 406 s. The FEM is also applied to solve the dynamic response of such mechanism for comparing the CPU time with the FDM. For the same case, the CPU time consumed to obtain the convergent result by using six elements and time step 5×10^{-5} s is

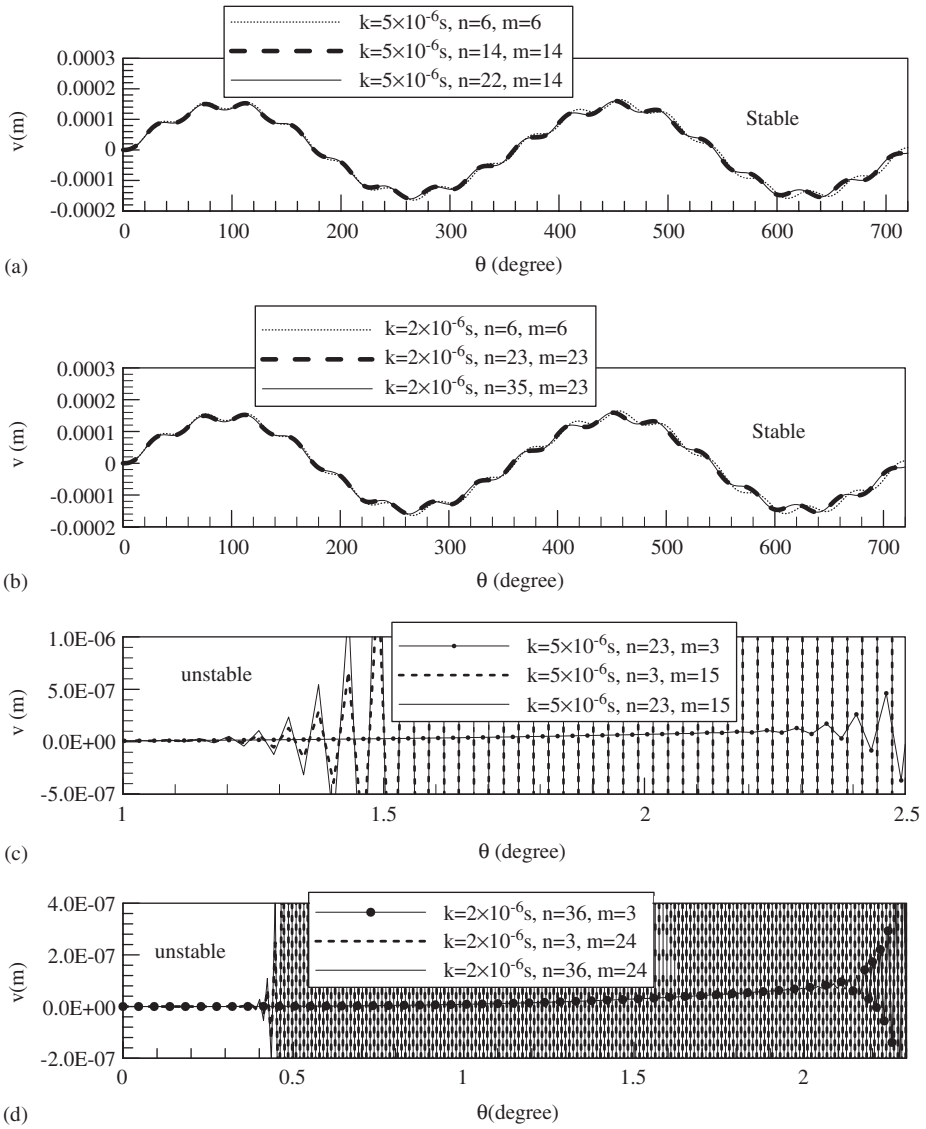

Fig. 6. Transverse deformations at the end point ($x = L$) with $m_{BC} = m_C = 0$ and $\dot{\theta} = 100\,\mathrm{rad/s}$ by using the variable-grid method.

Table 1
The stability conditions for various k and N_f by using the fixed-grid method

k	N_f	μ_f (Eq. (28))	Geometry constraint (Eq. (29))	Stable or unstable
5×10^{-6} s	12	0.0514	Satisfy	Stable
	24	0.2056	Satisfy	Stable
	36	0.4627	Satisfy	Stable
	10	0.0357	Violate	Unstable
	37	0.4888	Violate	Unstable
	38	0.5155	Violate	Unstable
2×10^{-6} s	12	0.0206	Satisfy	Stable
	36	0.1851	Satisfy	Stable
	59	0.4971	Satisfy	Stable
	10	0.0143	Violate	Unstable
	60	0.5141	Violate	Unstable

Table 2
The stability conditions for various k, n, and m by using the variable-grid method

K	N	m	μ_{v1} (Eq. (33))	μ_{v2} (Eq. (34))	Stable or unstable
5×10^{-6} s	3	3	0.0091	0.0207	Stable
	6	6	0.0364	0.0828	Stable
	14	14	0.1983	0.4507	Stable
	22	14	0.4898	0.4507	Stable
	23	3	0.5353	0.0207	Unstable
	3	15	0.0091	0.5174	Unstable
	23	15	0.5353	0.5174	Unstable
2×10^{-6} s	3	3	0.0036	0.0083	Stable
	6	6	0.0146	0.0331	Stable
	23	23	0.2141	0.4866	Stable
	35	23	0.4959	0.4866	Stable
	36	3	0.5246	0.0083	Unstable
	3	24	0.0036	0.5298	Unstable
	36	24	0.5246	0.5298	Unstable

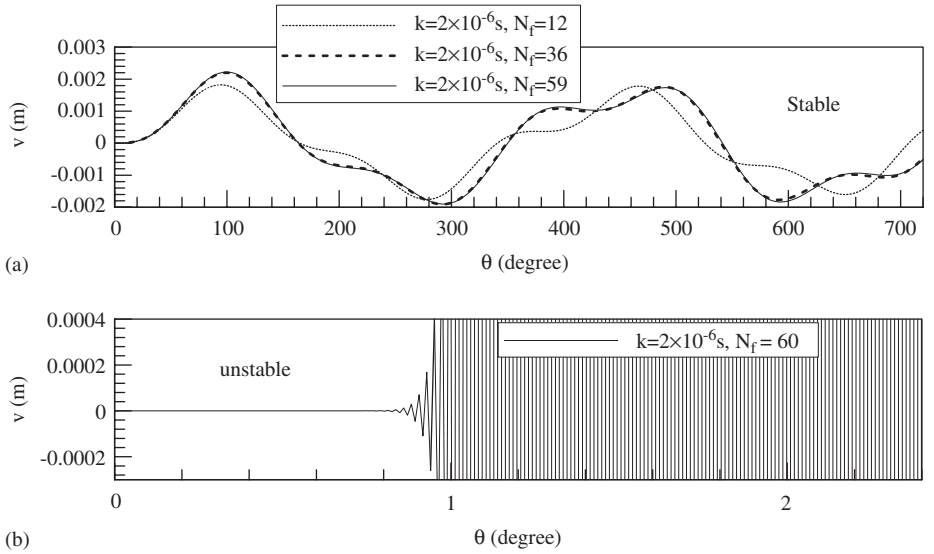

Fig. 7. Inertia effects of both rigid link BC and slider C on the deflections with $\dot{\theta} = 100\,\mathrm{rad/s}$ by using the fixed-grid method.

569 s. It is noted that the CPU time required using FDM is less than the FEM to obtain the convergent result. Especially, the fixed-grid method saves much more CPU time.

Figs. 7 and 8 compare the responses via the fixed- and variable-grid methods for the flexible quick-return mechanism considering the rigid link *BC* and slider *C*. It is seen from Figs. 7a and 8a that the convergent results via the fixed- and variable-grid methods are almost the same. Figs. 7b and 8b show the unstable deformations. The stability conditions for the case with and without considering the rigid link *BC* and slider *C* are all the same by comparing the results shown in Figs. 5–8. This means the stability conditions are irrelevant to boundary conditions for the studied mechanism. The transverse displacements for the mechanism while considering the rigid link *BC* and slider *C* are much larger than those without considering the rigid link *BC* and slider *C*.

5.2. The large crank case

The large crank problem differs from the small ones not only by the crank length, but also by the stiffness of the flexible rod. As the crank length increases, the steady-state responses increase [10]. The fixed-grid method

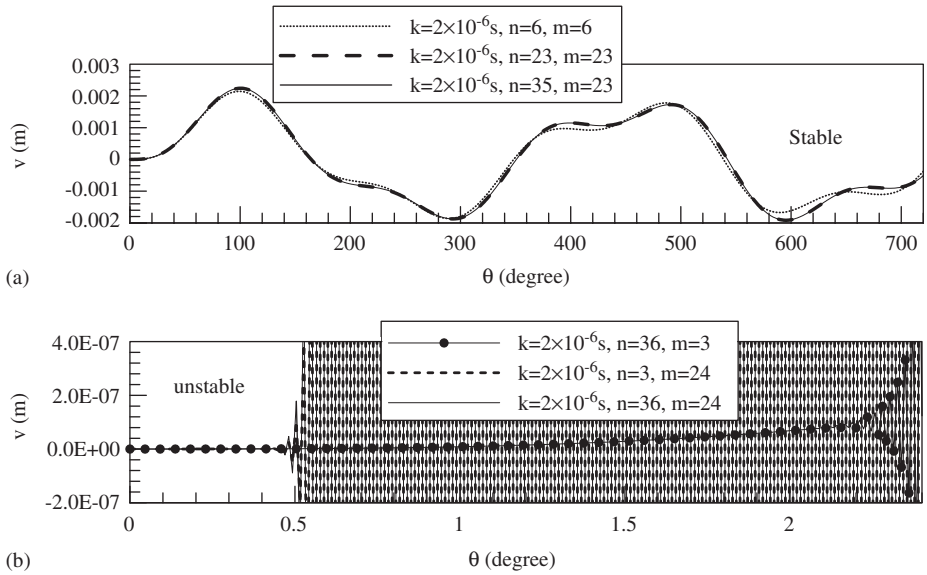

Fig. 8. Inertia effects of both rigid link BC and slider C on the deflections with $\dot{\theta} = 100\,\text{rad/s}$ by using the variable-grid method.

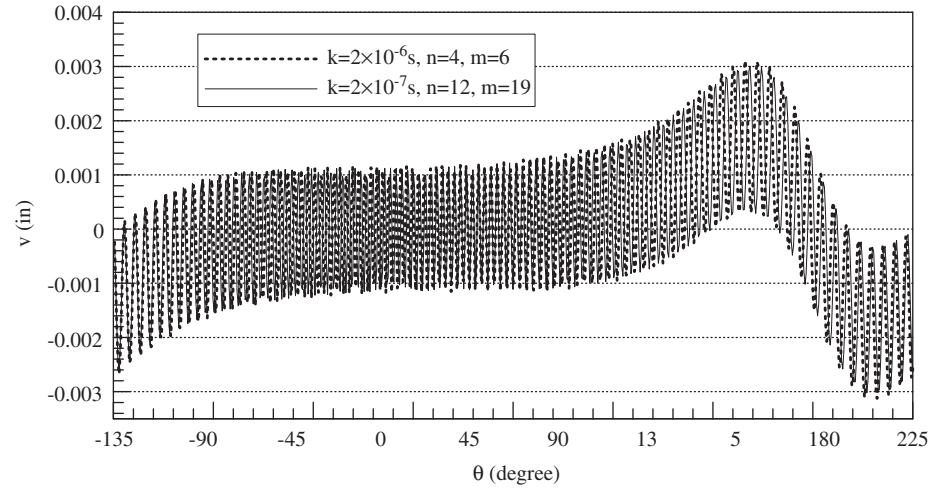

Fig. 9. Transverse deformations at the end point ($x = L$) for the case of the large crank and $\dot{\theta} = 90\,\text{rad/s}$ by using the variable-grid method.

fails for the large crank because the insurmountable numerical difficulties arise when a grid point comes close to the translating/rotating joint. The large crank has longer computation time required to run one cycle of the crank rotation compared to that of small crank.

The transverse deflection of the large crank is shown in Fig. 9. At time step $k = 2 \times 10^{-6}$ s, for satisfying the stability conditions, the largest n is 4 and m is 6. Since the limits of the space subdivision numbers are too small to get more accurate solutions, a finer time step is necessary to obtain better results, say $k = 2 \times 10^{-7}$ s. The limits of the space step number are $n = 12$ and $m = 19$ for $k = 2 \times 10^{-7}$ s. It is seen that there are high-frequency oscillations in the numerical results, and the transverse deformations are larger than those of the small crank case shown in Fig. 5. To gain an insight into the frequency response clearly, the time histories for first five consecutive cycles of Figs. 5 and 9 are transformed to frequency spectra by using the FFT, and the frequency spectra for the cases of the small crank and the large crank are shown in Figs. 10 and 11, respectively. It is seen from Fig. 10 that the transverse frequency responses have one significant peak and one small peak occurring near the harmonic and periodic-ten of angular speed of the crank, respectively. However,

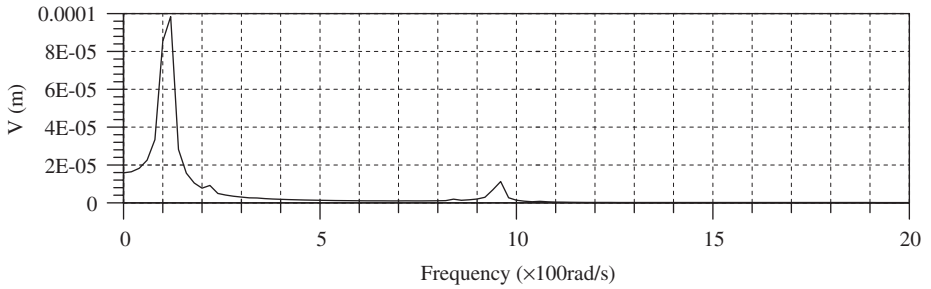

Fig. 10. The FFT spectra of transverse deformations at the end point ($x = L$) with $m_{BC} = m_C = 0$ and $\dot{\theta} = 100\,\text{rad/s}$ for the small crank.

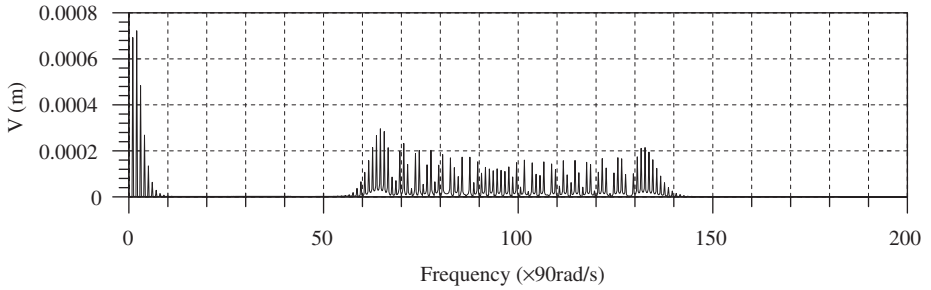

Fig. 11. The FFT spectra of transverse deformations at the end point ($x = L$) with $m_{BC} = m_C = 0$ and $\dot{\theta} = 90\,\text{rad/s}$ for the large crank.

for the large crank case as shown in Fig. 11, it is obvious to find the multiple peaks in the FFT spectra, the predominant peaks are located with angular speeds of the crank having periods 1 and 2 with the amplitude about 0.0007 m. The high-frequency peaks are integer multiples of the harmonic frequency, ranging from near 60 to near 140 times the angular speed of the crank with the largest amplitude about 0.0003 m. In the case studies, it is seen that the oscillation phenomena is much significant for the quick-return mechanism with the large crank. It is may be explained that the rigid-body motion and flexural vibration are severely coupled for the quick-return mechanism with the larger crank.

6. Discussion

From the FDM formulation and numerical simulations, the following observations are made:

(i) The loss of accuracy associated with singularities can arise when the moving boundary is too near a grid point. Some grid numbers, even though satisfying the stability condition, violate the geometry constraint due to the moving boundary. This is the major shortcoming of the finite difference scheme using the fixed grid.
(ii) In the variable-grid method, the speed and acceleration of the moving boundary introduced in the transformed equations reduce the storage and memory size requirements. The variable-grid method costs more computation time than the fixed-grid method.
(iii) In the fixed-grid method, the dynamic responses of the fixed nodal location obtained directly at any time provide an attractive feature for the control applications where point-sensor and point-actuators need to be placed at specified nodal points. However, it is difficult to find the transient results of the original node in the variable-grid method due to the coordinate transformation, which makes the node varying as the time increases.
(iv) Since the grids of two regions are in agreement, the fixed-grid method avoids the numerical difficulties associated with the continuity conditions at the moving boundary.

7. Conclusion

The flexible rod of a quick-return mechanism is modelled by Euler-beam theory. The calculus of variation and Hamilton's principle are used to derive the governing equations and boundary conditions. Due to the translating/rotating joint moving reciprocally along the flexible rod, the special FDMs with the fixed- and variable-grid schemes are proposed to approximate the numerical solutions. However, it is noticeable that numerical divergence occurs when the moving boundary moves across any of the neighboring nodes. Thus, the fixed-grid method is not applicable for the mechanism with the large crank. The possibility of singularities can be avoided via the variable-grid method, in which a coordinate transformation is employed to fix the moving boundary.

For a given time step, taking more space intervals can reduce the more numerical errors. To satisfy the stability and convergence conditions for the finite difference schemes, the number of space subdivision has an upper bound. Decreasing the time step can raise the upper bound of the number of space interval, however, leads to much computer time consumption.

It is impossible to find a method in which all the criteria are fulfilled. The choice of the numerical scheme depends not only on the nature of the problem but also on the priorities set by the user for accuracy, computation cost and ease of programming. As far as the above viewpoints are concerned, the following conclusions are drawn:

(i) The advantage of the FDMs employed in the quick-return mechanism is that it simplifies the process of the formulation and programming and conserves the accuracy of the solutions.
(ii) Galerkin's approach is too computationally intensive due to the time-dependent boundary and its complex mode shape.
(iii) Finite element techniques are time consuming and less amenable to vectorization than the FDMs, which continue to be widely used due to their simplicity in formulation and ease of programming.

Acknowledgements

The authors are greatly indebted to the National Science Council of ROC for the support of the research through contract no. NSC 89-2212-E-327-010.

Appendix A

By applying the FDM and Lagrange interpolation to the governing equations (12a, b), one can obtain $v_{i_r-1}^{j+1}$ and $v_{i_r+2}^{j+1}$ from the following two equations, respectively:

$$v_{i_r-1}^{j+1} = 2v_{i_r-1}^{j} - v_{i_r-1}^{j-1} - k^2 x_{i_r-1}\ddot{\phi}_j + k^2 v_{i_r-1}^{j}\dot{\phi}_j^2 - \frac{12EIk^2}{\rho Ah^4}\left(\frac{v_{i_r-3}^{j}}{3(p_j+3)} - \frac{v_{i_r-2}^{j}}{p_j+2} + \frac{v_{i_r-1}^{j}}{p_j+1} - \frac{v_{i_r}^{j}}{3p_j}\right), \tag{A.1}$$

$$v_{i_r+2}^{j+1} = 2v_{i_r+2}^{j} - v_{i_r+2}^{j-1} - k^2 x_{i_r+2}\ddot{\phi}_j + k^2 v_{i_r+2}^{j}\dot{\phi}_j^2 - \frac{12EIk^2}{\rho Ah^4}\left(\frac{v_{i_r+1}^{j}}{3(p_j-1)} + \frac{v_{i_r+2}^{j}}{2-p_j} + \frac{v_{i_r+3}^{j}}{p_j-3} + \frac{v_{i_r+4}^{j}}{3(4-p_j)}\right). \tag{A.2}$$

Concerning the boundary conditions (13c–f), the transverse displacements $v_{i_r-1}^{j}$ and $v_{i_r}^{j}$ can be found by solving the following equations simultaneously.

$$\frac{p_j-2}{1-p_j}v_{i_r+1}^{j} - \frac{p_j+1}{p_j}v_{i_r}^{j} = -\frac{p_j}{p_j+1}v_{i_r-1}^{j} + \frac{p_j-1}{2-p_j}v_{i_r+2}^{j}, \tag{A.3}$$

$$\frac{1}{1-p_j}v_{i_r+1}^{j} - \frac{1}{p_j}v_{i_r}^{j} = -\frac{1}{p_j+1}v_{i_r-1}^{j} + \frac{1}{2-p_j}v_{i_r+2}^{j}. \tag{A.4}$$

Appendix B

In region 1, $0 \leqslant x \leqslant x_1^-(t)$, the coordinate transformation (18) fixes the moving boundary at $\xi_1 = 1$ for all time and the governing equation (12a) becomes

$$\ddot{v}_1 - \frac{2\xi_1 \dot{x}_1}{x_1} \dot{v}_1' + \frac{\xi_1^2 \dot{x}_1^2}{x_1^2} v_1'' - \frac{\xi_1 (x_1 \ddot{x}_1 - 2\dot{x}_1^2)}{x_1^2} v_1' + \xi_1 x_1 \ddot{\phi} - \dot{\phi}^2 v_1 + \frac{EI}{\rho A x_1^4} v_1'''' = 0. \tag{B.1}$$

In region 2, $x_1^+(t) \leqslant x \leqslant L$, the coordinate transformation (19) fixes the moving boundary at $\xi_2 = 0$ for all time and Eq. (12b) becomes

$$\begin{aligned} \ddot{v}_2 + \frac{2(\xi_2 - 1)\dot{x}_1}{L - x_1} \dot{v}_2' + \frac{(\xi_2 - 1)^2 \dot{x}_1^2}{(L - x_1)^2} v_2'' + \frac{(\xi_2 - 1)[(L - x_1)\ddot{x}_1 + 2\dot{x}_1^2]}{(L - x_1)^2} v_2', \\ + [\xi_2 (L - x_1) + x_1]\ddot{\phi} - \dot{\phi}^2 v_2 + \frac{EI}{\rho A (L - x_1)^4} v_2'''' = 0. \end{aligned} \tag{B.2}$$

Reference

[1] S.N. Dwivedi, Application of Whitwork quick return mechanism for high velocity impacting press, *Mechanism and Machine Theory* 19 (1984) 51–59.

[2] D.G. Beale, R.A. Scott, The stability and response of a flexible rod in a quick return mechanism, *Journal of Sound and Vibration* 141 (2) (1990) 277–289.

[3] D.G. Beale, R.A. Scott, The stability and response of a flexible rod in a quick return mechanism: large crank case, *Journal of Sound and Vibration* 166 (3) (1993) 463–476.

[4] M.O. Okuyiga, W.H. Ray, Modelling and estimation for a moving boundary problem, *International Journal For Numerical Methods in Engineering* 21 (1985) 601–616.

[5] R.F. Fung, W.H. Cheng, Free vibration of a string/slider nonlinear coupling system, *Journal of the Chinese Society of Mechanical Engineers* 14 (1993) 229–239.

[6] H.P. Lee, Dynamics of a flexible rod in a quick return mechanism, *Transactions of the American Society of Mechanical Engineers, Journal Mechanical Design* 116 (1994) 70–74.

[7] B.M. Bahgat, K.D. Willmert, Finite element vibrational analysis of planar mechanisms, *Mechanism and Machine Theory* 11 (1976) 47–71.

[8] J.O. Song, E.J. Haug, Dynamic analysis of planar flexible mechanisms, *Computer Methods in Applied Mechanics and Engineering* 24 (1980) 359–381.

[9] Z. Yang, J.P. Sadler, Large-displacement finite element analysis of flexible linkages, *Transactions of the American Society of Mechanical Engineers, Journal of Mechanical Design* 112 (1990) 175–182.

[10] R.F. Fung, F.Y. Lee, Dynamic analysis of the flexible rod of a quick-return mechanism with time-dependent coefficients by the finite element method, *Journal of Sound and Vibration* 202 (2) (1997) 187–201.

[11] A. Shabana, B. Thomas, Chatter vibration of flexible multibody machine tool mechanisms, *Mechanism and Machine Theory* 22 (4) (1987) 359–369.

[12] R.F. Fung, K.W. Chen, Vibration Suppression and motion control of a non-linearly coupled flexible quick-return mechanism driven by a PM synchronous servo motor, *Journal of Sound and Vibration* 212 (4) (1998) 721–742.

[13] M. Stylianou, B. Tabarrok, Finite element analysis of an axially moving beam-Part I: time integration, *Journal of Sound and Vibration* 178 (1994) 433–453.

[14] B.O. Al-Bedoor, Y.A. Khulief, Finite element dynamic modeling of a translating and rotating flexible link, *Computer methods in applied mechanics and engineering* 131 (1996) 173–189.

[15] B.O. Al-Bedoor, Y.A. Khulief, General planar dynamics of a sliding flexible link, *Journal of Sound and Vibration* 206 (1997) 641–661.

[16] M. Zerroukat, C.R. Chatwin, *Computational Moving Boundary Problems*, Research Studies Press, England, 1994.

[17] J. Crank, *Free and Moving Boundary Problems*, Clarendon Press, Oxford, 1984.

[18] A. Kharab, Spreadsheet simulation of the moving boundary of the one-phase Stefan problem, *Computer Methods in Applied Mechanics and Engineering* 145 (1997) 217–225.

[19] P.C. Meek, J. Norbury, A two-stage, two-level finite difference scheme for moving boundary problems, *Computer Methods in Applied Mechanics and Engineering* 46 (1984) 137–149.

[20] R.S. Gupta, A. Kumar, Treatment of multi-dimensional moving boundary problems by coordinate transformation, *Journal of Heat Mass Transfer* 28 (7) (1985) 1355–1366.

[21] R.D. Richtmyer, K.W. Morton, *Difference Methods for Initial-Value Problems*, Wiley, New York, 1967.

[22] L. Gilles, S.C. Hagness, L. Vazquez, Comparison between staggered and unstaggered finite-difference time-domain grids for few-cycle temporal optical soliton propagation, *Journal of Computational Physics* 161 (2000) 379–400.